Proceedings of the ASME 2010 3rd Joint US-European Fluids Engineering Summer Meeting and 8th International Conference on Nanochannels, Microchannels, and Minichannels
FEDSM-ICNMM2010
August 1-5, 2010, Montreal, Canada

FEDSM-ICNMM2010-30431

AXIAL EVOLUTION OF ASYMMETRIC VORTICAL FLOW AROUND SLENDER BODY OF REVOLUTION AT HIGH INCIDENCE

Xiaorong Guan
School of Aerospace,
Tsinghua University
Beijing, China

Song Fu
School of Aerospace,
Tsinghua University
Beijing, China

Cheng Xu
School of Mechanical Engineering,
Nanjing University of Science and Technology
Nanjing, Jiangsu, China

ABSTRACT

For studying the axial evolution of the flow around slender body of revolution at high incidence under different conditions, numerical simulations are performed. Based on the computational results, several conclusions and deductions are obtained. When the flow is asymmetric and whether the asymmetry is remarkable or not, downstream axially it always presents itself in the structure of leeside vortices forming, rising and shedding alternately from opposite sides of the body and induces the sectional side force of waving sinusoidally. Based on the idea of vortex dividing, a forming mode of shed and new leeside vortices is put forward, which is composed of two idiographic manners. The axial evolutions on the forming manner can be reduced to three idiographic laws. The global asymmetry degree of the flow lies on both the axial evolution law on the forming manner and the intensity of leeside vortex. The influences of incidence, freestream Mach number and nose-perturbation location on the axial evolution of the asymmetric vortical flow are achieved as well.

Slender body of revolution; High-incidence aerodynamics; Asymmetric vortical flow

INTRODUCTION

The flow around slender body of revolution at incidence has been studied extensively for decades [1-6]. Since the flow is influenced simultaneously by lots of factors, it may appear in a wide variety of patterns and accordingly present distinct aerodynamic characteristics. For fully understanding the complicated flow, lots of studies have been carried out to study the influences of these factors [6-10].

With incidence increasing from 0º to 90º, the flow sequentially appears in steady attached pattern (in low incidence range), steady Symmetric Vortical Pattern (abbr., SVP, in middle incidence range), steady Asymmetric Vortical Pattern (abbr., AVP, in high incidence range) and unsteady vortical pattern (in extremely high incidence range) [4,11]. For the steady AVP is most complicated, uncertain and usually induces remarkable side force and yawing moment on the body even under zero sideslip condition, the flow at high incidence has become one of the most significant objects in the research field of aerodynamics.

With freestream Mach number increasing from zero, the global asymmetry degree of the flow at high incidence increases firstly and then decreases [2,7]. The most asymmetric flow appears under the condition of subsonic freestream, and the asymmetry nearly vanishes when freestream Mach number increases into the supersonic extent.

The flow at high incidence is highly sensitive to the perturbation located near nose apex (such as unavoidable minute imperfections produced in model machining) [9,10,12-14]. The nose perturbation may be directly responsible for the generation of the flow asymmetry, and it is just about the size and distribution randomness of nose-perturbation that results in the flow uncertainty.

Besides, lots of studies on the influences of the other factors (such as Reynolds number, nose configuration, etc.) have also been performed [15-17], and much valuable information has been obtained as well. Now, a question comes out naturally: are there any common or similar characteristics among the flows under different conditions? The primary objective of the current work is trying to answer it numerically, and several productions are achieved.

NOMENCLATURE

C_p	$=\left(p-p_\infty\right)/q$, surface-pressure coefficient
C_z	$=-\left(\int_0^{2\pi} p(\theta)\sin\theta \mathrm{d}\theta\right)/\left(2q\sin^2\alpha\right)$, coefficient of sectional side force
D	Diameter of cylindrical afterbody
H	Bump height
H_d	$=\left(\nabla\times\boldsymbol{V}\right)\cdot\boldsymbol{V}$, helicity density
L_A,L_N	Lengths of cylindrical afterbody, ogive nose
L_f	Distance between nose-bump forefront and nose apex
M_∞	Freestream Mach number
p, p_∞	Surface pressure, freestream pressure
q	$=\rho_\infty U_\infty^{\ 2}/2$, dynamic pressure

Re_D	$= U_\infty D \sin\alpha / \nu$, Reynolds number
U_∞	Freestream velocity
$\boldsymbol{V}$	Velocity vector
α, α_{AV}	Incidence, minimal incidence for flow asymmetry forming
γ	Circumferential angle of bump
θ	Azimuthal angle
v	Kinematic viscosity
ρ_∞	Freestream density

THEORETICAL BACKGROUND

Governing Equations and Numerical Algorithms

The conservation equations of mass, momentum and energy can be expressed generally in a conservative flux-vector form, which is convenient for numerical computation, i.e.,

$$\partial_\tau \hat{\boldsymbol{Q}} + \partial_{\xi}(\hat{\boldsymbol{F}} + \hat{\boldsymbol{F}}_v) + \partial_{\eta}(\hat{\boldsymbol{G}} + \hat{\boldsymbol{G}}_v) + \partial_{\zeta}(\hat{\boldsymbol{H}} + \hat{\boldsymbol{H}}_v) = 0 \qquad (1)$$

where the variables and flux vectors are well explained in Ref. [18].

A control-volume based method is employed to discretize the governing equations. The convection terms are discretized spatially with the MUSCL scheme, which can reduce numerical diffusions. The diffusion terms are discretized spatially with the second-order central-differencing scheme. The temporal discretization is implemented with a second-order fully-implicit scheme, which is unconditionally stable with respect to time-step size. For the flows of $M_\infty \le 0.2$, the SIMPLE algorithm is adopted to resolve the difficulty originated from the flow incompressibility; for the flows of $M_\infty > 0.2$, the above governing equations are solved simultaneously, and the Roe Flux-Difference Scheme is adopted to split the convection terms.

Turbulence Model

The coefficients of viscosity and thermal conductivity in the governing equations are given independently from auxiliary relations. The coefficients of molecular viscosity and turbulent viscosity are obtained respectively from the Sutherland's law and the SST k-ω turbulence model [19], which is suitable to outer flows and is accurate, reliable for both near-wall and far-field flow zones. The coefficient of thermal conductivity is obtained as the viscosity coefficient is known by assuming a constant Prandtl number. The discretization schemes adopted here are similar to those for the above governing equations, except that the convection terms are discretized spatially with a modified QUICK scheme, which can reduce numerical diffusions and is unconditionally stable.

Body Configurations and Computational Grids

The slender body of revolution consists of a 3D-long ogive nose (i.e., L_N=3D) and a 7D-long or 20D-long cylindrical afterbody (i.e., L_A=7D or 20D). They are tangentially jointed. A single geometric bump sketched in Fig. 1. is adopted to act as the nose perturbation, which was employed typically [10,14,20,21]. For simulating the minute imperfections lying objectively near nose apex of a physical model more closely, the bump size is of the same order as the physical surface roughness. The height is fixed at 0.0006D and 0.0009D respectively.

The computational outer boundary extends 12D radially from body surface and 10D (for subsonic flow) or 2D (for supersonic flow) axially in front of body (sketched in Fig. 2.). The computational grid is kept symmetric, aside from in a weeny zone around bump. The grid extending completely around the body consists of 120 circumferential planes. In each circumferential plane, the grid contains 60 radial points between body surface and computational outer boundary, and 85 (for L_A=7D) or 140 (for L_A=20D) axial points between nose apex and body rear. The circumferential grid planes are clustered properly in leeside of the body to resolve the vortices. The radial grid points are clustered properly near body surface to resolve the viscous layer. The minimal radial grid spacing near body surface is fixed at $10^{-5}D$ to assure a value of y^+<5 and to have at least 20 radial grid points within the viscous layer.

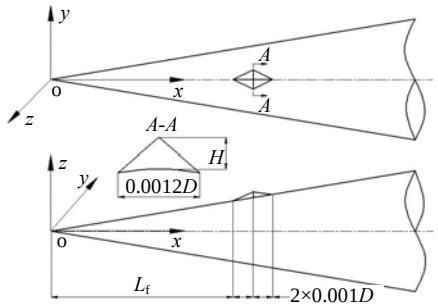

FIGURE 1. SKETCH OF MINUTE NOSE BUMP AND COORDINATE SYSTEM FOR DATA PROCESSING.

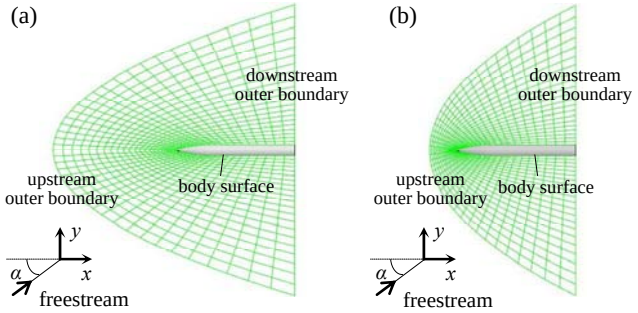

FIGURE 2. SKETCH OF SOLUTION DOMAIN AND GRID: (a) SUBSONIC FLOW, (b) SUPERSONIC FLOW.

Boundary Conditions and Initial Conditions

An adiabatic no-slip condition is maintained on the body surface. Namely, all the velocity components on the body surface and the total heat flux through the body surface are zero. A characteristic condition is kept at the computational outer boundary: at the upstream, the freestream values are specified; at the downstream, for the type of governing equations changes with M_∞ increasing from subsonic into supersonic extent, the non-reflected condition is applied for subsonic flows and the extrapolation condition is applied for supersonic flows instead [22]. A periodic continuation condition is enforced at the circumferential grid edges.

When performing a computation, the entire flowfield is initially set to the freestream condition throughout the grid or to a previously obtained one. A global-constant time step is employed for time-dependent computation, and the solution is marched in time until a quasi-steady flowfield is achieved.

COMPUTATIONAL RESULTS AND DISCUSSIONS

All computations are performed for α ranged from 25° to 60°, M_∞ ranged from 0.01 to 2.2 and Re_D ranged from 6.8×10^4 to 1.5×10^7. In addition, all computations are turbulent by respectively setting the freestream turbulence intensity and turbulent viscosity ratio to 1.0% and 1.0.

Conventions for Data Processing

The right-handed coordinate system sketched in Fig. 1. is adopted, where the origin is located at the nose apex, and the x axis is aligned with the principal axis. The orientations of "left" and "right" appearing below are defined with respect to plane z=0 as looking along the positive x direction. The "symmetric" and "asymmetric" are also defined with respect to plane z=0. Both θ=0° and γ=0° are fixed at the windward sideline of the fore-and-aft symmetric plane of the body, and their positive directions are both defined anticlockwise as looking along the positive x direction.

Examinations of Computational Results

It has been validated in Ref. [14] that the numerical methods and flow models adopted here are suitable for the current study and the computational results are fairly reliable. Since the slender body has two types of L_A, several additional computations are performed to examine the effect of L_A on the computational results near forebody, and a quantitative agreement (demonstrated in Fig. 3.) is achieved. It indicates that the computational results obtained from different L_As can be united together to perform uniform study.

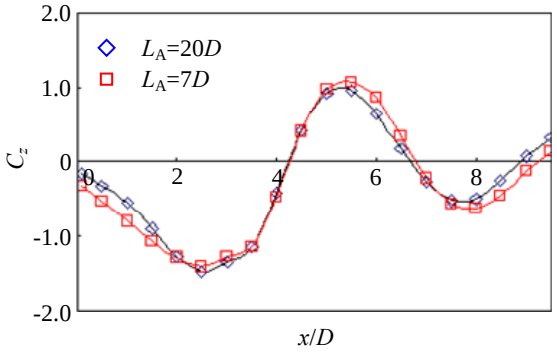

FIGURE 3. EFFECT OF L_A ON AXIAL EVOLUTION OF C_z, H=0.0006D, L_f=0.022D, γ=90°, α=50°, M_∞=0.2, Re_D=1.4×10^6.

Typical Flow Patterns

All the flow patterns obtained here can be classified into two quasi-steady types (except for micro-amplitude and high-frequency unsteadiness in shear layer): SVP and AVP. As α<30º, the flow always appears in SVP; as α≥30º, the flow is likely to appear in AVP instead. It indicates that α_{AV} is about 30º in the current work, which is consistent with the previous results [7,8,23]. That's to say, the high incidence range starts at about 30º here.

On the premise of $\alpha \geq \alpha_{AV}$, without nose perturbation, the flow always remains symmetric; when nose perturbation is appended, the flow usually turns to remarkably asymmetric promptly; further as nose perturbation is removed again, the flow returns to symmetric. It shows that the flow is highly sensitive to the nose perturbation, which is in good agreement with both the earlier experimental and numerical results [9,10,13]. Thus it can be seen that two conditions are necessary for the flow to appear in AVP: one is $\alpha \geq \alpha_{AV}$, and the other is proper perturbations existing near nose apex.

When the flow appears in SVP, two nose vortices run almost parallel to the body upper surface as growing downstream (illustrated in Fig. 4. (a)). For convenience, the vortex forming on leeside of the body due to the primary separation of boundary layer is named leeside vortex, and further the two leeside vortices rooting near nose apex (i.e., V_{L1} and V_{R1}) are named nose vortices. The symmetric structure induces symmetric aerodynamic characteristics. The circumferential distribution of C_p at any axial location is approximately symmetric (demonstrated in Fig. 5. (a)), and the sectional side force at any axial location is almost zero (demonstrated in Fig. 6.).

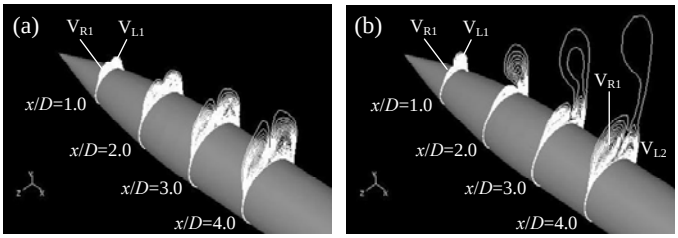

FIGURE 4. CONTOUR MAPS OF $|H_d|$ [24], L_A=7D, α=50º, M_∞=0.2, Re_D=1.4×10^6: (a) NO BUMP, (b) H=0.0006D, L_f=0.006D, γ=90°.

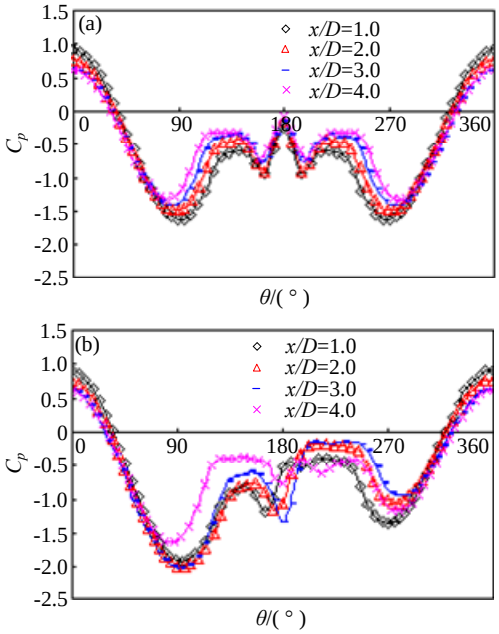

FIGURE 5. CIRCUMFERENTIAL DISTRIBUTIONS OF C_p, L_A=7D, α=50º, M_∞=0.2, Re_D=1.4×10^6: (a) NO BUMP, (b) H=0.0006D, L_f=0.006D, γ=90°.

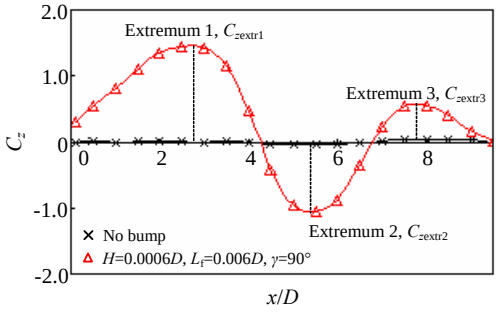

FIGURE 6. AXIAL EVOLUTIONS OF C_z, L_A=7D, α=50º, M_∞=0.2, Re_D=1.4×10^6.

As the flow appears in remarkable AVP, it is obvious that it shows itself in the structure of leeside vortices forming, rising and shedding alternately from opposite sides of the slender body downstream axially (illustrated in Fig. 4. (b)) and induces remarkably lateral aerodynamic characteristics (illustrated in Fig. 5. (b) and 6.).

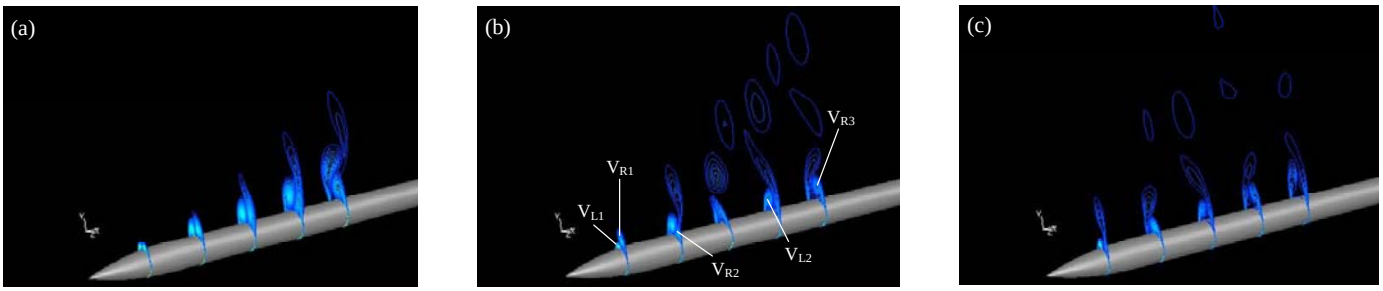

FIGURE 7. CONTOUR MAPS OF $|H_d|$ AT x/D=2.0/4.0/6.0/8.0/10.0 AT DIFFERENT αS, L_A=20D, H=0.0006D, L_f=0.022D, γ=90º, M_∞=0.2: (a) α=38°, Re_D=2.7×10^5, (b) α=50°, Re_D=3.3×10^5, (c) α=60°, Re_D=3.8×10^5.

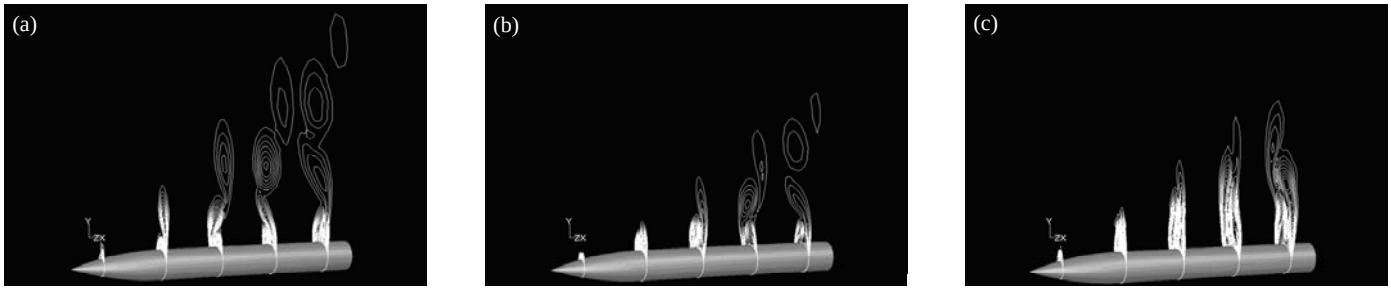

FIGURE 8. CONTOUR MAPS OF $|H_d|$ AT x/D=1.0/3.0/5.0/7.0/9.0 UNDER DIFFERENT M_∞S, L_A=7D, H=0.0006D, γ=90º, α=50º: (a) L_f=0.022D, M_∞=0.2, Re_D=1.4×10^6, (b) L_f=0.022D, M_∞=0.6, Re_D=4.1×10^6, (c) L_f=0.014D, M_∞=1.2, Re_D=8.1×10^6.

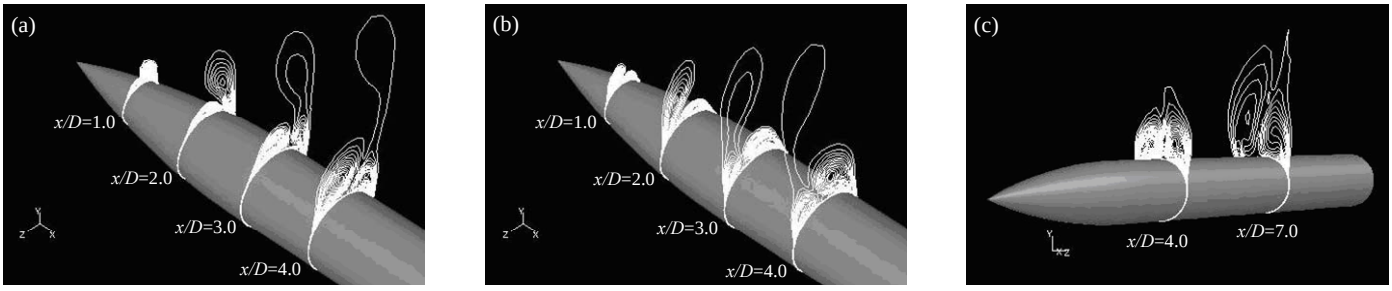

FIGURE 9. CONTOUR MAPS OF $|H_d|$ UNDER DIFFERENT PERTURBATION CONDITIONS, L_A=7D, γ=90º, α=50º, M_∞=0.2, Re_D=1.4×10^6: (a) H=0.0006D, L_f=0.006D, (b) H=0.0006D, L_f=0.022D, (c) H=0.0009D, L_f=0.009D.

For the inducement of leeside vortex on body surface mainly lies on its intensity and distance away from body surface, variational intensity and/or variational distance lead to variational inducement and further variational negative pressure on body surface [25]: with leeside vortex intensifying and/or the distance decreasing, the inducement strengthens and further the negative pressure increases. Therefore, when V_{L1} rises firstly downstream axially, its inducement weakens and further the negative pressure on body surface of left side decreases (illustrated in Fig. 5. (b)); at the same time, for V_{R1} keeps close to body surface, its inducement strengthens a little due to its intensity increasing, and further the negative pressure on body surface of right side increases a little. It is just about the negative-pressure difference on opposite sides that leads to the generation of sectional side force (illustrated in Fig. 6.). Downstream axially, along with leeside vortices forming, rising and shedding alternately from opposite sides of the body, the difference sign of negative pressure on opposite sides is alternate, and consequently the sectional side force waves sinusoidally.

Axial Evolution of Asymmetric Vortical Flow

The asymmetric flow pattern at high incidence is influenced by many factors, so with flow conditions changing, it is uncertain and may be quite different from the remarkable AVP presented above. However, several common or similar characteristics among the flows under different conditions are observed. It is deduced from the flow structures obtained numerically here (such as illustrated in Fig. 7. to 9.) that, as long as the flow appears in AVP and whether the asymmetry is remarkable or not, downstream axially it always presents itself in the structure of leeside vortices forming, rising and shedding alternately from opposite sides of the body.

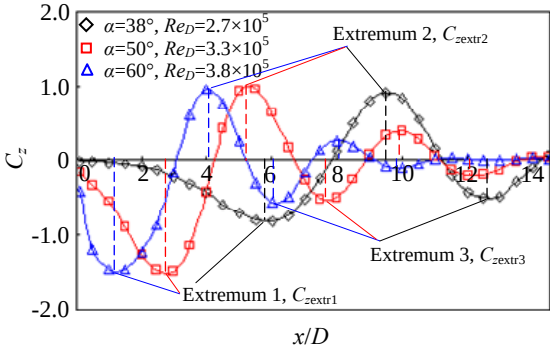

FIGURE 10. AXIAL EVOLUTIONS OF C_z AT DIFFERENT αS, L_A=20D, H=0.0006D, L_f=0.022D, γ=90º, M_∞=0.2.

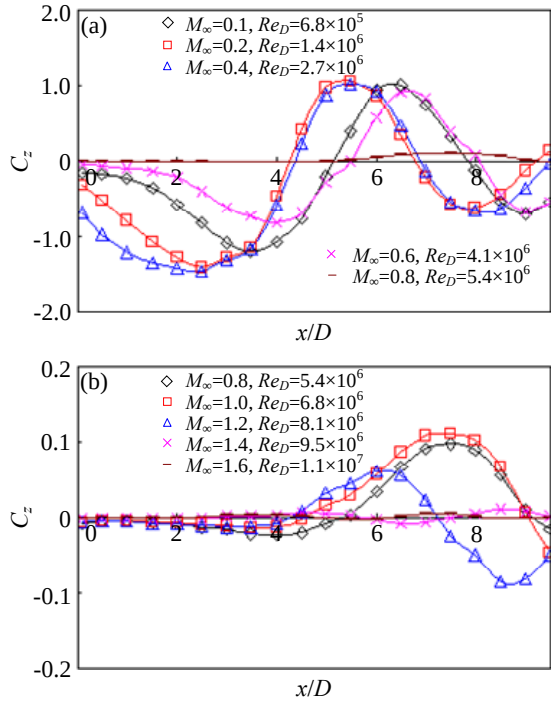

FIGURE 11. AXIAL EVOLUTIONS OF C_z UNDER DIFFERENT M_∞S, L_A=7D, H=0.0006D, L_f=0.022D, γ=90º, α=50º: (a) $M_\infty \le 0.8$, (b) $M_\infty \ge 0.8$.

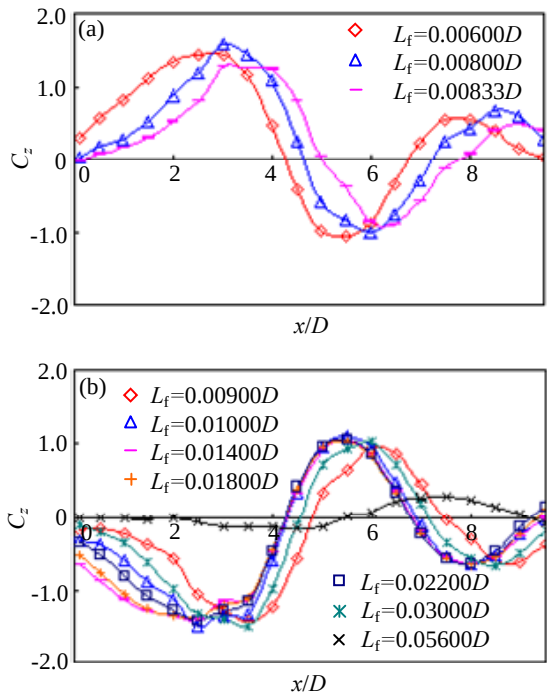

FIGURE 12. AXIAL EVOLUTIONS OF C_z UNDER DIFFERENT L_fS, L_A=7D, H=0.0006D, γ=90º, α=50º, M_∞=0.2, Re_D=1.4×10^6: (a) L_f<0.00867D, (b) L_f>0.00867D.

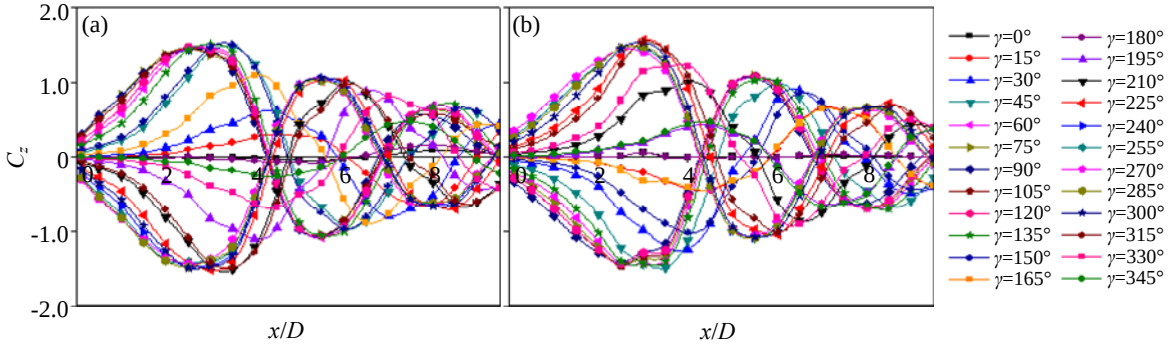

FIGURE 13. AXIAL EVOLUTIONS OF C_z UNDER DIFFERENT γS, L_A=7D, H=0.0006D, α=50º, M_∞=0.2, Re_D=1.4×10^6: (a) L_f=0.006D, (b) L_f=0.022D.

Maybe under some conditions, it is hard to distinguish such a structure (such as illustrated in Fig. 9. (c)), while the structure can still be inferred from the axial evolution of C_z. When the flow appears in AVP and whether the asymmetry is remarkable or not, C_z always waves sinusoidally downstream axially (such as illustrated in Fig. 10. to 13.). As is discussed above, such a situation is just an image of the flow structure that leeside vortices form, rise and shed alternately from opposite sides of the body downstream axially.

However, it should be accepted that there are notable differences among the flows under different conditions. For example, the axial pace of leeside vortices forming, rising, shedding as well as the size of shed vortex is different obviously (demonstrated in Fig. 7. to 9.); the axial phase as well as the amplitude of C_z waving is naturally different obviously (demonstrated in Fig. 10. to 13.). Why on earth do these differences exist? For answering it, the forming mode of shed and new leeside vortices is to be discussed firstly.

Forming Mode of Shed and New Leeside Vortices

How on earth do shed and new leeside vortices form in the asymmetric flow around slender body of revolution at high incidence? Based on the computational results obtained in the current work, an opinion founded on the idea of vortex dividing is advanced. It includes two idiographic manners: (1) secondary vortex extruding and dividing primary vortex on same side; (2) lower-lying vortex extruding and dividing higher-lying vortex on opposite side. In AVP, there is always a pair of leeside vortices attaching body surface at any cross section. For convenience, the one staying farther away from body surface is named higher-lying vortex (such as V_{R1} at x/D=4.0 in Fig. 4. (b)) and the other is named lower-lying vortex (such as V_{L2} at x/D=4.0 in Fig. 4. (b)). Two examples are taken here to respectively explain these two idiographic manners: Ex.1 – L_A=20D, H=0.0006D, L_f=0.022D, γ=90º,

α=50º, M_∞=0.2, Re_D=3.3×10^5; Ex.2 – L_A=20D, H=0.0006D, L_f=0.022D, γ=90º, α=38º, M_∞=0.2, Re_D=2.7×10^5.

Secondary Vortex Dividing Primary Vortex on Same Side Ex.1 is used here. Downstream axially, nose vortices V_{L1} and V_{R1} induce secondary separations to form secondary vortices V_{LS} and V_{RS} respectively; with V_{LS}, V_{RS} expanding and intensifying by degrees, V_{L1} and V_{R1} are respectively extruded and divided into two parts (illustrated in Fig. 14.). For convenience, the above parts are denoted with the symbols for the original primary vortices and the lower parts are denoted with V_{LT}, V_{RT} respectively. With V_{R1} keeping rising, the separated shear layer doesn't provide vorticity for V_{R1} any more, and V_{R1} goes on rising to become the first shed vortex; subsequently, the downstream separated shear layer on the right side begins to convolute around V_{RT} to form the new leeside vortex V_{R2}. Hereto, V_{L1} becomes the new higher-lying vortex and V_{R2} grows into the new lower-lying vortex. For convenience, this manner is named Manner A. It is obvious that the secondary separation is a necessary condition for Manner A. It can be seen that vortices V_{LT} and V_{RT} are just the tertiary vortices advanced by Wang et al. [26], and Manner A is in accord with the experimental phenomenon that tertiary vortex evolves to form new leeside vortex.

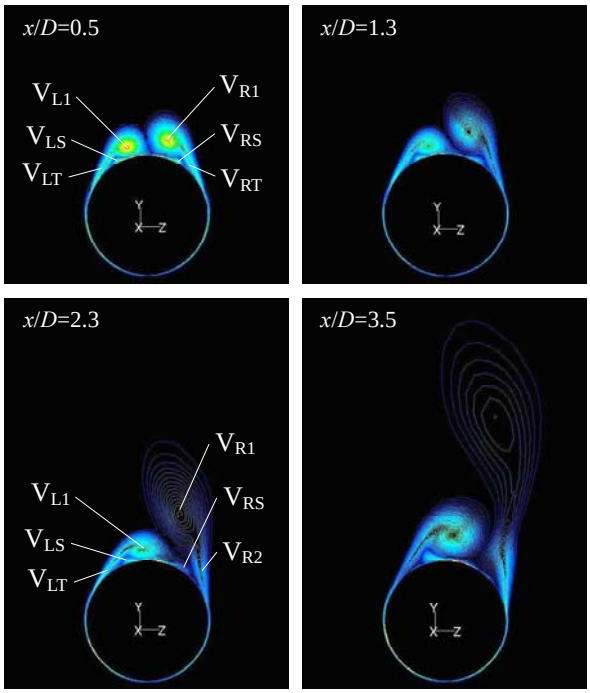

FIGURE 14. CONTOUR MAPS OF $|H_d|$, L_A=20D, H=0.0006D, L_f=0.022D, γ=90º, α=50º, M_∞=0.2, Re_D=3.3×10^5.

Lower-Lying Vortex Dividing Higher-Lying Vortex on Opposite Side Ex. 2 is used here. Downstream axially, with V_{L1} and V_{R1} intensifying, they also induce secondary separations to form secondary vortices V_{LS}, V_{RS} respectively. With V_{LS} and V_{RS} expanding and intensifying, V_{L1} and V_{R1} are also extruded and divided into two parts respectively (illustrated in Fig. 15.). While in this case, the formation of shed vortex V_{R1} has nearly nothing to do with the secondary and tertiary vortices, which is distinct from the instance discussed above. That's to say, the secondary separation is not a necessary condition for Manner B.

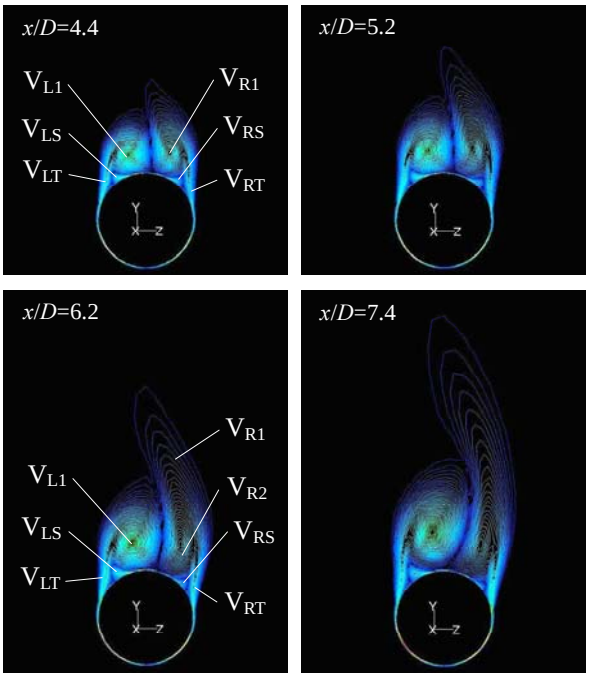

FIGURE 15. CONTOUR MAPS OF $|H_d|$, L_A=20D, H=0.0006D, L_f=0.022D, γ=90º, α=38º, M_∞=0.2, Re_D=2.7×10^5.

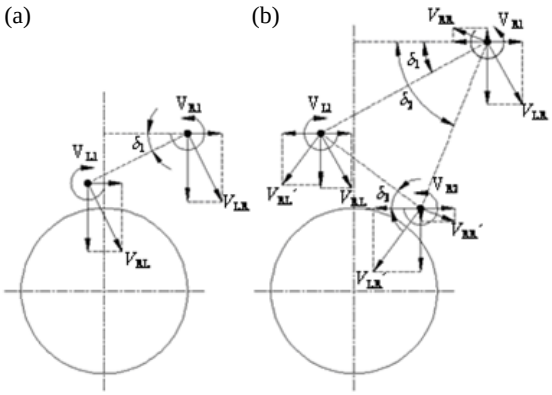

FIGURE 16. INDUCEMENTS OF LEESIDE VORTICES [25]: (a) ASYMMETRIC TWO LEESIDE VORTICES, (b) ASYMMETRIC THREE LEESIDE VORTICES.

Downstream axially, with V_{R1} rising, for the lateral component of the inducement velocity of V_{R1} on V_{L1} directs right (i.e., $|\boldsymbol{V}_{RL}|\sin\delta_1$ illustrated in Fig. 16. (a)), V_{L1} begins to shift right and extrude V_{R1} in the middle. After developing in the axial extent of SVP near nose apex, V_{L1} has expanded and intensified a lot when V_{R1} begins to rise (illustrated in Fig. 7. (a)), so the position of V_{L1} extruding V_{R1} is higher and the inducement of V_{L1} on V_{R1} is relatively strong. At the same time, for the upright component of the inducement velocity of V_{L1} on V_{R1} (i.e., $|\boldsymbol{V}_{LR}|\cos\delta_1$) directs downwards, the rise of V_{R1} is restrained. It can be seen from Fig. 15. that V_{R1} just rises a little. The lesser height difference between V_{L1} and V_{R1} means that δ_1 is lesser and $|\boldsymbol{V}_{LR}|\cos\delta_1$ is biggish, so the rise of V_{R1} is restrained strongly. Simultaneously, for the directions of $|\boldsymbol{V}_{LR}|\cos\delta_1$ and the "entrainment" of mainstream are contrary and V_{R1} is extruded by V_{L1} from side at a higher position, V_{R1} elongates (along y direction) by degrees. In the course of V_{R1} rising slowly and elongating by degrees, V_{L1} also rises

gradually. With V_{L1} expanding, intensifying and shifting right further, its extrusion on V_{R1} strengthens further. Since the vorticity signs of V_{L1} and V_{R1} are contrary, when the extrusion of V_{L1} on V_{R1} reaches a certain extent, V_{R1} is divided into two parts: the above part doesn't absorb vorticity any more and goes on rising to become the first shed vortex V_{R1} (i.e., denoted with the symbol for the original primary vortex); the lower part keeps on absorbing vorticity from separated shear layer to grow into the new leeside vortex V_{R2}. Hereto, V_{L1} becomes the new higher-lying vortex, and V_{R2} grows into the new lower-lying vortex. For convenience, it is named Manner B, and the proportions of the vorticity above and below the dividing point to the whole vorticity of the original higher-lying vortex are signed with $r_{\omega u}$ and $r_{\omega d}$ respectively. Under different conditions, as the shed and new leeside vortices are formed with Manner B, $r_{\omega u}$ and $r_{\omega d}$ are variational.

Axial Evolution on Forming Manner of Shed and New Leeside Vortices

It can be inferred that, when higher-lying vortex is too weak to induce secondary separation or the induced secondary vortex is too weak, the shed and new leeside vortices can just be formed with Manner B. Besides, as the height difference between higher-lying and lower-lying vortices is lesser, the shed and new leeside vortices are also usually formed with Manner B: for lower-lying vortex has strong restraint on higher-lying vortex rising, the higher-lying vortex can just rise a little and keeps absorbing vorticity from separated shear layer; simultaneously, for lower-lying vortex has strong extrusion and division effect on higher-lying vortex and lastly divides higher-lying vortex into two parts. When shed and new leeside vortices are formed with Manner B, the less the height difference is, the smaller $r_{\omega u}$ is and the bigger $r_{\omega d}$ is, further the weaker the shed vortex is and the more intensive the new lower-lying vortex is initially. Contrarily, when the height difference is biggish, the shed and new leeside vortices are usually formed with Manner A instead.

The asymmetric structures of leeside vortices forming, rising and shedding alternately from opposite sides of the body downstream axially are all implemented with the combinations of Manner A and B. For example, the asymmetric structure of Ex.1 is implemented with the combination A-A-B-B-B, while the asymmetric structure of Ex.2 is implemented with the combination B-A-B-B-B instead. Why on earth are the asymmetric structures under different conditions implemented with different combinations of Manner A and B?

The upright components of inducement velocities of lower-lying and shed vortices on higher-lying vortex both direct downwards (such as $|\boldsymbol{V}_{RL}'|\cos\delta_3$, $|\boldsymbol{V}_{RL}|\cos\delta_1$ illustrated in Fig. 16. (b)), and they restrain the rise of higher-lying vortex obviously; while the higher-lying vortex can still rise by degrees. It indicates that the "entrainment" of the mainstream is decisive to the rise of leeside vortex, which is consistent with the experimental phenomenon that the locomotion trails of all shed vortices went to the mainstream direction lastly [25]. That's to say, though the upright components of inducement velocities of higher-lying and shed vortices on lower-lying vortex both direct downwards (such as $|\boldsymbol{V}_{LR}'|\cos\delta_3$, $|\boldsymbol{V}_{RR}'|\cos\delta_2$), the lower-lying vortex can still rise (demonstrated in Fig. 14. and 15.). Downstream axially, with the distances between shed and lower-lying vortices increasing one by one and leeside vortices weakening one by one, the downward components of inducements of shed and higher-lying vortices on lower-lying vortices decrease one by one, so the restraints on lower-lying vortices rising weakens one by one and further the rising scopes of lower-lying vortices have the trend of increasing one by one, which means that the height differences between higher-lying and lower-lying vortices have the trend of decreasing one by one. As a result, downstream axially, the forming manners of shed and new leeside vortices have the trend of transforming from A to B or $r_{\omega u}$s minishing one bye one, which is the first type of trend here.

It can be inferred from the asymmetric structure of Ex. 2 that, downstream axially, if there is an obvious axial extent of SVP existing near nose apex, the first shed and new leeside vortices will be formed with Manner B; the longer the axial extent of SVP is, the bigger and the more intensive the lower-lying vortex is at the beginning of flow asymmetry appearing, so the higher the position of lower-lying vortex dividing higher-lying vortex is, and the smaller $r_{\omega u}$ is when the first shed and new leeside vortices are formed. Downstream axially, through the regulation of the forming process of the first shed and new leeside vortices, the influence of the axial extent of SVP near nose apex on the forming manners of downstream shed and new leeside vortices weakens, and the forming manners of downstream shed and new leeside vortices have the trend of transforming to Manner A, which is the second type of trend here. The bigger $r_{\omega u}$ is when the first shed and new leeside vortices are formed, the more possibly the downstream shed and new leeside vortices are formed with Manner A.

Thus, the axial evolution on forming manner of shed and new leeside vortices is influenced simultaneously by the above two distinct types of trends. If there is no obvious axial extent of SVP existing near nose apex (such as Ex. 1), the first shed and new leeside vortices will be formed with Manner A, and the forming manners of downstream shed and new leeside vortices will transform from A to B ($r_{\omega u}$s in Bs will decrease one by one). While if there is an obvious axial extent of SVP existing near nose apex, the first shed and new leeside vortices will be formed with Manner B, and the axial evolution on forming manner of downstream shed and new leeside vortices will have two possibilities: (1) as the obvious axial extent of SVP is lesser (such as Ex.2), the forming manners will transform to A firstly ($r_{\omega u}$s in Bs maybe will increase one by one firstly) and then back to B ($r_{\omega u}$s in Bs will decrease one by one); (2) as the obvious axial extent of SVP is biggish (such as illustrated in Fig. 9. (c)), all the shed and new leeside vortices will be formed with Manner B ($r_{\omega u}$s in Bs will increase firstly and then decrease one by one). The first type of trend is the nature of the flow, while the second type lies on the obvious axial extent of SVP near nose apex, so the axial evolution on forming manner of shed and new leeside vortices mainly lies on whether the obvious axial extent of SVP near nose apex exists and how long it is. It can be drawn that with the obvious axial extent of SVP near nose apex elongating from zero by degrees, the axial evolution on forming manner of shed and new leeside vortices will sequentially appear in: (1) law χ — from Manner A to B gradually ($r_{\omega u}$s in Bs will decrease one by one); (2) law λ — from Manner B to A firstly ($r_{\omega u}$s in Bs maybe will increase one by one firstly) and then back to B ($r_{\omega u}$s in Bs will decrease one by one); (3) law μ — Manner B all through ($r_{\omega u}$s in Bs will increase firstly and then decrease one by one).

Correlations between Aerodynamic Characteristics and Flow Structures

Since secondary and tertiary vortices are much smaller and weaker than primary vortices, their influences on the aerodynamic characteristics are usually ignored [25].

Distribution of Sectional-Side-Force Extremum It was usually considered that the sectional side force of waving sinusoidally always reached an extremum downstream axially just as a shed vortex was formed [3]. Namely, an extremum point was just corresponding to a vortex-shedding point. While distinct phenomenon

has been observed in the current work: downstream axially, the formation of C_{zextri} (i=1, 2, 3, ⋯, the ith extremum of sectional-side-force coefficient) always lags behind the formation of the ith shed vortex (demonstrated in Fig. 17.), which is consistent with the experimental results in Ref. [25]. That's to say, downstream axially, the flow asymmetry will keep on increasing after a vortex shedding fresh. Why on earth does the phenomenon happen?

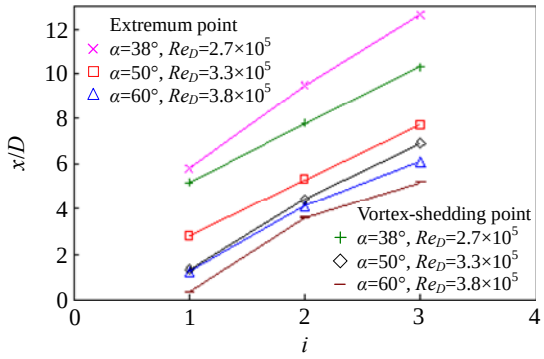

FIGURE 17. AXIAL DISTRIBUTIONS OF C_{zextr}S AND VORTEX-SHEDDING POINTS, L_A=20D, H=0.0006D, L_f=0.022D, γ=90°, M_∞=0.2.

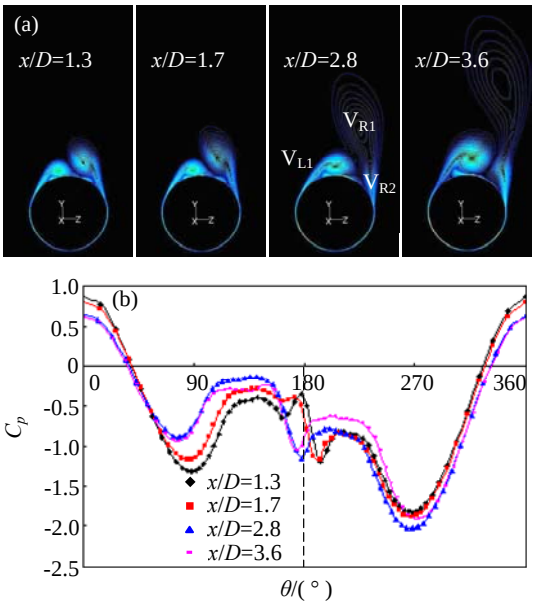

FIGURE 18. FORMING PROCEDURE OF C_{zextr1}, L_A=20D, H=0.0006D, L_f=0.022D, γ=90°, α=50°, M_∞=0.2, Re_D=3.3×10^5: (a) CONTOUR MAPS OF $|H_d|$, (b) CIRCUMFERENTIAL DISTRIBUTIONS OF C_p.

C_{zextr1} of Ex.1 is taken here to present the forming procedure of a C_{zextr} (illustrated in Fig. 18.). Downstream with V_{R1} rising firstly, the negative pressure on body surface of right side begins to decrease. The emergence of the negative-pressure difference between opposite sides leads to the generation of a non-zero C_z, which directs towards the side of lower-lying vortex V_{L1} (illustrated in Fig. 10.). With V_{R1} keeping on rising, the height difference between V_{R1} and V_{L1} increases, which leads the negative-pressure difference to increase, so C_z increases. At about x/D=1.3, the first shed vortex V_{R1} and new leeside vortex V_{R2} are formed with Manner A. With V_{R1} rising further, its inducement on body surface weakens further; with V_{R2} intensifying due to absorbing vorticity from separated shear layer, its inducement on body surface strengthens. At the beginning, the strengthening scope of inducement on body surface due to V_{R2} intensifying can not compensate the weakening scope due to V_{R1} rising further, so the negative pressure on body surface of right side decreases further; simultaneously, though V_{L1} has begun to rise, the strengthening scope of its inducement on body surface due to intensifying is high enough to compensate the weakening scope due to rising, so the total inducement of V_{L1} on body surface keeps strengthening and the negative pressure on body surface of left side keeps increasing. As a result, the negative-pressure difference increases further and C_z goes on increasing.

Downstream axially further, with V_{R2} keeping absorbing vorticity to intensify, the strengthening scope of its inducement on body surface gradually approaches, reaches and lastly exceeds the weakening scope due to V_{R1} rising up further (in the course, the inducement of V_{R1} becomes secondary), and the negative pressure on body surface of right side turns from decreasing to increasing; at the same time, with V_{L1} rising up further, the weakening scope of its inducement on body surface duo to rising gradually approaches, reaches and lastly exceeds the strengthening scope due to intensifying, so the negative pressure on body surface of left side turns from increasing to decreasing. Thus, the difference of negative pressure turns from increasing to decreasing gradually. In the course, C_{zextr1} is formed at about x/D=2.8 axially.

Thus it can be seen that the reason for flow asymmetry keeping increasing downstream after a vortex shedding fresh includes two aspects, in the beginning period of a shed vortex forming: (1) the strengthening scope of inducement on body surface due to new leeside vortex intensifying can still not compensate the weakening scope due to shed vortex keeping rising, so the negative pressure on body surface of shed-vortex side decreases further; (2) the strengthening scope of inducement on body surface due to higher-lying vortex intensifying is higher than the weakening scope due to rising further, so the negative pressure on body surface of the opposite side of shed vortex increases further. That's to say, in the beginning period of a shed vortex forming, the negative pressure on body surface of the side where the negative pressure is higher will increase further, while the negative pressure on body surface of the side where the negative pressure is lower will decrease further, so the negative-pressure difference between opposite sides will increase and naturally C_z will increase further. This is the main reason for that the formation of C_{zextri} always lags behind the formation of the ith shed vortex downstream axially.

Magnitude of Sectional-Side-Force Extremum The magnitude order of C_{zextr}s distributed downstream axially is uncertain: when α=50º and 60º, $|C_{zextr1}|>|C_{zextr2}|>|C_{zextr3}|$; however, when α=38º, $|C_{zextr1}|<|C_{zextr2}|$ and $|C_{zextr2}|>|C_{zextr3}|$ instead (illustrated in Fig. 10.). Since the aerodynamic characteristics are the exterior reflections of the flow structure, for mastering the magnitude order, the study should also be started from analyzing the flow structure.

It can be considered that Manner A is a special case of Manner B, where $r_{\omega d}$=0, so these two manners can be discussed uniformly with Manner B. The higher the position of lower-lying vortex dividing higher-lying vortex is, the smaller $r_{\omega u}$ is, the lower the weakening scope of inducement on body surface is due to shed vortex rising, the smaller the loss of negative pressure on body surface of shed-vortex side is; simultaneously, higher position of lower-lying vortex dividing higher-lying vortex indicates that the rising scope of lower-lying vortex is higher, so the restraint on the strengthening scope of inducement on body surface due to lower-lying vortex intensifying is stronger and the increase scope of negative pressure on body surface of lower-lying-vortex side is smaller. Thus it can be seen that the

higher the position of lower-lying vortex dividing higher-lying vortex is, the smaller the negative-pressure difference between opposite sides is in the course of shed and new leeside vortices forming, the smaller the magnitude of $C_{z\text{extr}}$ is. In addition, the magnitude of $C_{z\text{extr}}$ is also impacted by the intensity of leeside vortices: the weaker the leeside vortices are, the smaller the possible biggest magnitude of $C_{z\text{extr}}$ is. Downstream, for leeside vortices always weaken one by one, from the aspect of leeside-vortex intensity, the magnitudes of $C_{z\text{extr}}$s have the trend of decreasing one by one. It means that the uncertainty of the magnitude order of $C_{z\text{extr}}$s distributed downstream mainly lies on the uncertainty of the heights of lower-lying vortex dividing higher-lying vortex in the axial evolution of the asymmetric vortical structure.

When the axial evolution on forming manner of shed and new leeside vortices appears in law χ, the positions of lower-lying vortex dividing higher-lying vortex heighten one by one downstream, so from both the aspects of the height of vortex dividing and the vortex intensity, the magnitudes of $C_{z\text{extr}}$s will decrease one by one. Ex.1 is such a case (demonstrated in Fig. 10.). While the axial evolution appears in law λ or μ, the positions of lower-lying vortex dividing higher-lying vortex lower firstly and then heighten downstream, and thus the magnitude order of $C_{z\text{extr}}$s is uncertain. For example, in Ex.2, in the course of $C_{z\text{extr1}}$ forming, for the position of V_{L1} dividing V_{R1} is higher (illustrated in Fig. 15.), though the vortices are stronger, the magnitude of $C_{z\text{extr1}}$ is still smaller; in the course of $C_{z\text{extr2}}$ forming, for the position of V_{R2} dividing V_{L1} lowers obviously, though the vortices are weaker, the magnitude of $C_{z\text{extr2}}$ still grows larger; downstream further, in the course of downstream extrema forming, for both leeside vortices weaken and the positions of lower-lying vortex extruding and dividing higher-lying vortex heighten one by one, the magnitudes of downstream extrema minish one by one.

Thus it can be seen that, for neighbor $C_{z\text{extr}i}$ and $C_{z\text{extr}(i+1)}$, the magnitude of $C_{z\text{extr}(i+1)}$ is smaller doubtless from the aspect of vortex intensity. At the same time, if the position of lower-lying vortex dividing higher-lying vortex heightens downstream, the magnitude of $C_{z\text{extr}(i+1)}$ is also smaller from the aspect of vortex dividing, so it is sure that the magnitude of $C_{z\text{extr}(i+1)}$ is smaller; however, if the position lowers downstream, the magnitude of $C_{z\text{extr}(i+1)}$ is larger from the aspect of vortex dividing instead, so the relative magnitude between $C_{z\text{extr}i}$ and $C_{z\text{extr}(i+1)}$ is uncertain and mainly lies on the relative magnitude between the decrease scope of C_z due to leeside vortices weakening and the increase scope due to the position of lower-lying vortex dividing higher-lying vortex lowering: if the former is lager, the magnitude of $C_{z\text{extr}(i+1)}$ is smaller; if the latter is larger, the magnitude of $C_{z\text{extr}(i+1)}$ is larger instead.

In sum, it can be drawn that: (1) relatively to induced by the case of shed and new leeside vortices formed with Manner A, the asymmetry induced by the case of formed with Manner B is weaker, and with $r_{\omega\text{u}}$ decreasing, the asymmetry decreases; (2) with the axial evolution on forming manner of shed and new leeside vortices transforming from law χ to λ and then to μ, the global flow asymmetry decreases; viz., with the obvious axial extent of SVP near nose apex elongating from zero, the global flow asymmetry decreases.

It should be supplied that the global flow asymmetry will not increase infinitely. The asymmetry degree lies on both the height of lower-lying vortex dividing higher-lying vortex and vortex intensity: with the height lowering and/or vortex intensifying, the asymmetry strengthens. So with the obvious axial extent of SVP near nose apex shortening and vanishing lastly: (1) the height decreases by degrees, and the flow asymmetry has the trend of increasing; (2) the axial pace of leeside vortices forming, rising and shedding alternately from opposite sides of the body downstream quickens, and the axial extent of leeside vortices intensifying through absorbing vorticity from separated shear layer shortens, so the flow asymmetry has the trend of decreasing. Namely, the above two distinct trends in one course insure that the flow asymmetry will not increase infinitely and will reach a saturation state under a special balance between these two trends, which is consistent with previous experimental phenomena [9,12,13].

Influences of Factors on Axial Evolution of Asymmetric Vortical Flow

Incidence With α increasing from α_{AV}, the obvious axial extent of SVP near nose apex shortens by degrees and vanishes lastly, so the axial evolution on forming manner of shed and new leeside vortices appears in law μ, λ and χ sequentially and the global flow asymmetry strengthens gradually (demonstrated in Fig. 7. and 10.).

Freestream Mach Number With M_∞ increasing, the flow sequentially appears in subsonic, transonic and supersonic patterns. As the flowfield is completely subsonic, M_∞ is subcritical; otherwise, M_∞ is supercritical. In the current work, the critical value is in between 0.4 and 0.5.

With M_∞ increasing gradually in the subcritical extent, the obvious axial extent of SVP near nose apex shortens by degrees and vanishes lastly, so the axial evolution on forming manner of shed and new leeside vortices sequentially appears in law μ, λ, χ and the global flow asymmetry strengthens gradually (demonstrated in Fig. 11.).

When M_∞ increasing into the supercritical extent and increasing further, the obvious axial extent of SVP near nose apex comes into being afresh and elongates gradually, so the axial evolution on forming manner of shed and new leeside vortices transforms back from law χ to λ and then to μ. When M_∞ is larger than 0.8, $r_{\omega\text{u}}$s in law μ have become very minute (illustrated in Fig. 8. (c)). In the course, the global flow asymmetry weakens gradually and becomes very weak when M_∞ is larger than 1.2 (demonstrated in Fig. 11.).

Nose-Perturbation Location With nose perturbation shifting closer to both circumferential and axial critical locations [14] or farther away from nose apex gradually, the obvious axial extent of SVP near nose apex elongates from zero by degrees, so the axial evolution on form manner of shed and new leeside vortices sequentially appears in law χ, λ, μ and the global flow asymmetry weakens gradually (demonstrated in Fig. 12. and 13.).

CONCLUSIONS

A numerical study is performed to investigate the axial evolution of the flow around slender body of revolution at high incidence under different conditions. Based on the computational results and the correlative qualitative analysis, several conclusions as well as deductions are achieved.

(1) When the flow appears in AVP and whether the asymmetry is remarkable or not, it always presents itself in the structure of leeside vortices forming, rising and shedding alternately from opposite sides of the body downstream axially, and always induces the sectional side force of waving sinusoidally.

(2) A forming mode of shed and new leeside vortices is put forward. It is composed of two idiographic manners: Manner A – secondary vortex extruding and dividing primary vortex on same side; Manner B – lower-lying vortex extruding and dividing higher-lying vortex on opposite side.

(3) All the asymmetric vortical flows are implemented with the combinations of Manner A and B. With the obvious axial extent of SVP near nose apex elongating from zero, the axial evolution on forming manner of shed and new leeside vortices sequentially appears in: law χ — from Manner A to B; law λ — from Manner B to A firstly and then back to B; law μ — Manner B all through.

(4) Downstream axially, the formation of C_{zextri} always lags behind the formation of the *i*th shed vortex. The extremum magnitude lies on both the height of lower-lying vortex dividing higher-lying vortex on opposite side and vortex intensity. With the obvious axial extent of SVP near nose apex elongating from zero, the global flow asymmetry weakens gradually.

(5) With α increasing from α_{AV} or M_∞ increasing in subcritical extent by degrees, the obvious axial extent of SVP near nose apex shortens and vanishes lastly, so the axial evolution on forming manner of shed and new leeside vortices sequentially appears in law μ, λ, χ and the global flow asymmetry strengthens gradually; with M_∞ increasing in supercritical extent, nose perturbation shifting closer to both axial and circumferential critical locations or farther away from nose apex, the variation directions of both flow structures and aerodynamic characteristics are converse.

These conclusions as well deductions can provide elicitation and reference for the future study on the asymmetric flow around slender body of revolution at high incidence. Accordingly, for enhancing the reliability and persuasion, it is necessary for the future to validate them further with numerical results from higher accuracy approaches (such as LES), experimental results and quantitative analysis. Additionally, in order to verify their universality, further studies should be carried out for the flows in more situations.

ACKNOWLEDGMENTS

Thank the reviewers for their valuable suggestions. Thank the colleagues in Lab for Advanced Simulation of Turbulence, Tsinghua University and 105 Research Lab, Nanjing University of Science and Technology for their help in discussion and text proofreading.

REFERENCES

[1] Allen, H. J., and Perkins, E. W., 1951, "Characteristics of Flow over Inclined Bodies of Revolution," NACA RMA50L07.

[2] Thomson, K. D., and Morrison, D. F., 1971, "The Spacing, Position and Strength of Vortices in the Wake of Slender Cylindrical Bodies at Large Incidence," J. Fluid Mech., 50(4), pp. 751-783.

[3] Lamont, P. J., and Hunt, B. L., 1976, "Pressure and Force Distributions on a Sharp-Nosed Circular Cylinder at Large Angles of Inclination to a Uniform Subsonic Stream," J. Fluid Mech., 76(3), pp. 519-559.

[4] Ericsson, L. E., and Reding, J. P., 1985, "Aerodynamic Effects of Asymmetric Vortex Shedding from Slender Bodies," AIAA Paper No. 1985-1797.

[5] Liu, P. Q., and Deng, X. Y., 2002, "Lee-Side Vortex Structure and Aerodynamic Characteristics Analysis over a Slender Cylinder at High Incidence," Acta Mech. Sin., 34(2), pp. 248-255.

[6] Wang, G., Liang, X. G., and Deng, X. Y., 2004, "Effects of Roll Angle on Side Force Distribution over Slender Bodies of Revolution at High Angle of Attack," Exp. Meas. Fluid Mech., 18(4), pp. 11-14.

[7] Keener, E. R., Chapman, G. T., and Kruse, R. L., 1976, "Effects of Mach Number and Afterbody Length on Aerodynamic Side Forces at Zero Sideslip on Symmetric Bodies at High Angles of Attack," AIAA Paper No. 1976-0066.

[8] Lamont, P. J., 1985, "The Effect of Reynolds Number on Normal and Side Forces on Ogive-Cylinders at High Incidence," AIAA Paper No. 1985-1799.

[9] Moskovitz, C. A., Dejarnette, F. R., and Hall, R. M., 1989, "Effects of Nose Bluntness, Roughness and Surface Perturbations on the Asymmetric Flow past Slender Bodies at Large Angles of Attack," AIAA Paper No. 1989-2236.

[10] Degani, D., 1990, "Numerical Investigation of the Origin of Vortex Asymmetry," AIAA Paper No. 1990-0593.

[11] Wang, G., Deng, X. Y., Wang, Y. K., and Chen, X. R., 2003, "Zonal Study of Flow Patterns around an Ogive-Cylinder at Subcritical Reynolds Numbers," Exp. Meas. Fluid Mech., 17(2), pp. 19-25+36.

[12] Degani, D., and Zilliac, G. G., 1990, "Experimental Study of Nonsteady Asymmetric Flow around an Ogive-Cylinder at Incidence," AIAA J., 28(4), pp. 642-649.

[13] Dexter, P. C., and Hunt, B. L., 1981, "The Effect of Roll Angle on the Flow over a Slender Body of Revolution at High Angles of Attack," AIAA Paper No. 1981-0358.

[14] Guan, X. R., Xu, C., Wang, Y. J., and Wang, Y. P., 2009, "Influence of Nose-Perturbation Location on Behavior of Vortical Flow around Slender Body at High Incidence," Sci. China Ser. E - Tech. Sci., 52(7), pp. 1933-1946.

[15] Hall, R. M., 1987, "Influence of Reynolds Number on Forebody Side Forces for 3.5-Diameter Tangent-Ogive Bodies," AIAA Paper No. 1987-2274.

[16] Ericsson, L. E., 1988, "Effect of Nose Bluntness and Cone Angle on Slender-Vehicle Transition," AIAA J., 26(10), pp. 1168-1174.

[17] Howard, R. M., Lung, M. H., and Rabang, M. P., 1991, "Effects of Freestream Turbulence on Asymmetric Vortex Formation over a Tangent-Ogive Forebody," AIAA Paper No. 1991-0290.

[18] Viviand, H., 1974, "Conservative Forms of Gas Dynamics Equations," La Recherche Aerospatiale, (1), pp. 65-68.

[19] Menter, F. R., 1994, "Two-Equation Eddy-Viscosity Turbulence Models for Engineering Applications," AIAA J., 32(8), pp. 1598-1605.

[20] Yang, Y. J., Cui, E. J., and Zhou, W. J., 2004, "Numerical Studies about Asymmetric Vortex Flow around a Slender Body at High Incidence," Acta Mech. Sin., 36(1), pp. 1-8.

[21] Degani, D., and Levy, Y., 1992, "Asymmetric Turbulent Vortical Flows over Slender Bodies," AIAA J., 30(9), pp. 2267-2273.

[22] Hwang, S. J., and Rho, O. H., 1995, "Numerical Simulation of Asymmetric Vortical Flows on a Slender Body at High Incidence," AIAA Paper No. 1995-1799.

[23] Reding, J. P., and Ericsson, L. E., 1978, "Maximum Vortex-Induced Side Force," J. Spacecr. Rockets, 15(4), pp. 201-207.

[24] Levy, Y., Degani, D., and Seginer, A., 1990, "Graphical Visualization of Vortical Flows by Means of Helicity," AIAA J., 28(8), pp. 1347-1352.

[25] Wang, G., 2002, "Experimental Study of Flowfield Structure around an Ogive-Cylinder," Ph.D. thesis, Beihang University, Beijing.

[26] Wang, G., Liang, X. G., and Deng, X. Y., 2004, "Formation of Tertiary Vortex and Dynamical Process of Vortices Asymmetric around a Slender Body," J. Tsinghua Univ. (Sci. & Tech.), 44(8), pp. 1120-1125.